Arsenic, Copper, and Zinc Leaching through Preferential Flow in Mining-Impacted Soils

Martin Helmhart
Institute for Agricultural Sciences
Consejo Superior de Investigaciones Científicas
Serrano 115-dup
28006 Madrid, Spain

Peggy A. O'Day
School of Natural Sciences
Univ. of California-Merced
5200 N. Lake Rd.
Merced, CA 95343

Javier Garcia-Guinea
National Museum of Natural Sciences
Consejo Superior de Investigaciones Científicas
Jose Gutierrez Abascal 2
28006 Madrid, Spain

Susana Serrano
Fernando Garrido*
Institute for Agricultural Sciences
Consejo Superior de Investigaciones Científicas
Serrano 115-dup
28006 Madrid, Spain

The effect of preferential flow on the spatial distribution of As, Cu, and Zn and chemical speciation of As was studied within the surface riverbed (RB) layer of a small stream that collects surface runoff from an As-bearing waste pile of an abandoned mine. Water flow domains, preferential (PF) or matrix (MF), were identified by staining techniques. In-stream soils had lower pH and higher As, Cu, Zn, and Fe concentrations than soils outside the stream channel. Mean metal(loid) concentrations were higher in RB samples than in the subsoil (SS), but no strong correlations were found in the RB between metal(loids) and either PF or MF, with the exception of Zn and MF paths. In contrast, in the SS, PF paths were associated with lower Cu and Zn concentrations and higher concentrations of As, extractable Fe, and total organic C compared with MF soils. Analysis of SS samples by As x-ray absorption spectroscopy (XAS) indicated that As was present only as arsenate sorbed to Fe(III) oxide phases, and Fe XAS showed a higher proportion of ferrihydrite, in addition to illite–smectite, in a PF than a MF sample. Results indicate an overall transport of contaminants and Fe from storage in RB soils, where flow regimes are heterogeneous, into the SS as a result of acid leaching. In the SS, preferential flow domains act as conduits for transport of Cu and Zn into the soil matrix but retain As heterogeneously through sorption on amorphous Fe(III) oxides that may dissolve and precipitate within macropores.

Abbreviations: ECEC, effective cation exchange capacity; EXAFS, extended x-ray absorption fine structure; GLZ, generalized linear model; ICP–AES, inductively coupled plasma–atomic emission spectrometry; MF, matrix flow; PF, preferential flow; RB, riverbed; SS, subsoil; TOC, total organic carbon; XANES, x-ray absorption near edge structure; XAS, x-ray absorption spectroscopy; XRD, x-ray diffraction.

The fate and mobility of As and other hazardous metals in soils impacted by mining wastes are influenced by coupled biogeochemical processes that control the element oxidation state, mineral surface sorption and desorption, and solid-phase precipitation and dissolution. Knowledge of the mechanisms that control contaminant release, mobility, and natural attenuation is crucial to minimize the risk and consequences associated with mine wastes (Cheng et al., 2009; Johnson and Hallberg, 2005). The role that inhomogeneous infiltration and wetting front instabilities leading to preferential flow (PF) phenomena play on the distribution and solid speciation and transport of As and other metals in soils affected by acid mine drainage (AMD) is less well studied, however. Preferential flow is the rapid movement of water and solutes through soils that bypasses large portions of the soil matrix and thus affects a small fraction of the soil volume (Hagedorn and Bundt, 2002). Flow through structural macropores such as soil fissures, cracks, root channels, or earthworm burrows are the main causes for PF (Jarvis, 2007). In sandy soils, fingering can occur (Lennartz et al., 2008) due to

Soil Sci. Soc. Am. J. 76:449–462
Posted online 9 Dec. 2011
doi:10.2136/sssaj 2011.0269
Received 27 July 2011
*Corresponding author (fernando.garrido@ica.csic.es)

trapped air or changes in soil texture or water repellency (Lipsius and Mooney, 2006), producing those eponymous fingers.

Overall, these phenomena have been shown to reduce the sorbing capacity of the soil and the residence time of solutes, which may lead to a significant increased risk of groundwater contamination from soil leaching (Lipsius and Mooney, 2006). For instance, the role of PF in increasing metal transport has been shown in undisturbed soil columns (Camobreco et al., 1996). In field conditions, the effect of PF has also been described for the enhanced transport of radionuclides (Bundt et al., 2000), pesticides (Ghodrati, 1992), nutrients (Toor et al., 2005; Seo and Lee, 2005), dissolved organic matter (Bundt et al., 2001a), and Pb (Knechtenhofer et al., 2003). The physicochemical properties of the PF paths may be different than those of the surrounding soil matrix, however, which may result in different microbial activity (Bundt et al., 2001b), C and N dynamics (Bundt et al., 2001a), or metal retention capacity due to differences in organic matter content (Bundt et al., 2001c). Moreover, differences in chemical or mineralogical properties associated with PF or matrix flow (MF) within the soil may also induce differences in metal(loid) retention mechanisms and, subsequently, in potential bioavailability and leachability.

While the occurrence of PF is recognized as a common field phenomenon (Morales et al., 2010), further research is needed to reveal whether nonequilibrium water flow conditions may effectively control metal distribution and retention mechanisms in the soil and to elucidate the mechanisms behind the transport of metals through the soil, especially in locations affected by large amounts of metals released due to AMD. This study aimed to describe the effect of PF phenomena on As, Cu, and Zn spatial distributions at the pedon scale in a small catchment area affected by AMD and high concentrations of toxic elements. Specifically, our objectives were (i) to identify flow domains within the riverbed and underlying soil profile, (ii) to test whether PF phenomena control metal(loid) distribution in the soil profile, (iii) to investigate multi-elemental associations and their spatial distribution within PF and MF flow domains, and (iv) to investigate differences in As speciation and metal distribution in soils as a function of different flow domains.

MATERIALS AND METHODS

Experimental Site and Soil Characteristics

The experiment was conducted in shrub land situated in the upper area of a small subcatchment of the Guadalix River (Madrid, Spain) feeding the Madrid Tertiary Detrital Aquifer. Arsenopyrite (FeAsS) and scorodite ($FeAsO_4 \cdot 2H_2O$) are found in association with S^{2-}–bearing pegmatite outcrops in this area (Recio-Vazquez et al., 2011). The site includes an abandoned smelting factory in which arsenopyrite encapsulated in quartz was processed for wolfram extraction during the Second World War. The mining wastes, containing up to 190 g kg^{-1} of As, were and currently remain dumped on the soil surface (Recio-Vazquez et al., 2011), thus subjected to erosion and weathering processes (Fig. 1A).

The experimental plot was situated in a leveled portion within the riverbed of a small stream (~1 m wide) that seasonally collects surface runoff from the As-bearing waste pile (Fig. 1B). Four 60-cm-depth undisturbed soil cores (5 cm in diameter) were taken from the experimental plot for general characterization (Fig. 1B). Two of them were taken within the riverbed (in-stream cores) and the other two were collected ~1 m from the stream edge (out-stream cores). In the laboratory, the cores were cut at 10-cm intervals. Each soil portion was air dried, homogenized, and sieved (2-mm mesh) before analysis (Table 1). Previous spectroscopic experiments showed the absence of Fe(II) in both soil layers (data not shown). In addition, no hydromorphic reducing conditions were found in the soil columns as they were dismantled in the laboratory after sampling the treatment under anoxic conditions. The texture was determined by the pipette method after

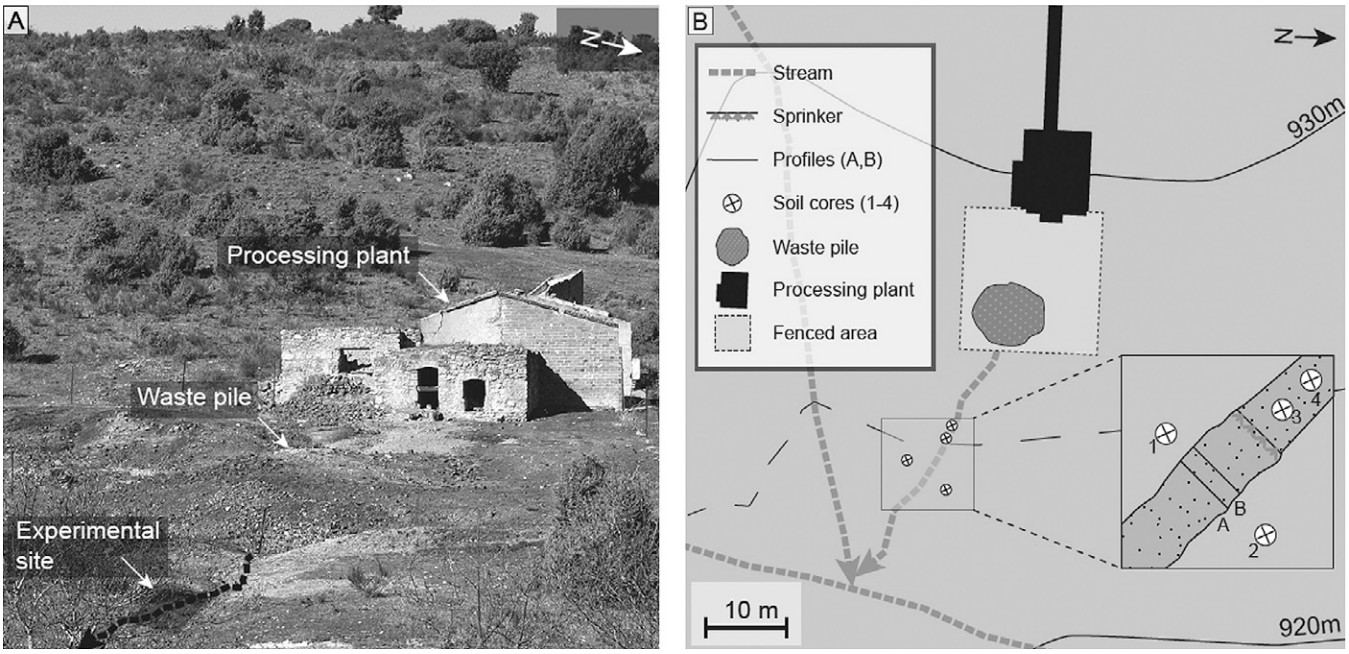

Fig. 1. (A) An abandoned processing plant with waste pile in the foreground, and (B) schematic plan of the study site.

Table 1. Physical, mineralogical, and chemicals properties of out-stream and in-stream soil cores (mean values from corresponding columns).

Depth	Sand	Silt	Clay	TOC†	pH_w‡	pH_K‡	EC§	Exchangeable cations				
								Ca^{2+}	Mg^{2+}	Na^{2+}	K^+	Al^{3+}
cm	%						$\mu S\ cm^{-1}$	$cmol_c\ kg^{-1}$				
Out-stream soil cores												
0–10	21	45	34	0.5	7.8	5.6	223	3.6 ± 0.03¶	1.4 ± 0.01	1.1 ± 0.03	0.3 ± 0.005	<0.01
10–20	17	47	37	0.1	8.3	6.4	443	4.2 ± 0.04	1.7 ± 0.02	2.0 ± 0.06	0.3 ± 0.005	<0.01
20–30	17	47	37	0.1	8.7	6.9	680	3.6 ± 0.03	1.7 ± 0.02	2.4 ± 0.08	0.3 ± 0.005	<0.01
30–40	23	45	32	0.1	8.4	7.2	1139	4.2 ± 0.04	1.6 ± 0.02	2.0 ± 0.06	0.3 ± 0.005	<0.01
40–50	28	43	30	0.1	8.6	7.2	996	2.6 ± 0.02	1.5 ± 0.02	2.0 ± 0.06	0.2 ± 0.003	<0.01
50–60	27	41	32	0.1	8.7	7.2	1074	3.0 ± 0.03	1.6 ± 0.02	2.3 ± 0.07	0.2 ± 0.003	<0.01
In-stream soil cores												
0–10	49	31	21	0.9	5.2	3.9	177	0.5 ± 0.005	0.1 ± 0.001	0.1 ± 0.001	0.6 ± 0.006	0.9 ± 0.009
10–20	47	32	22	0.8	4.6	3.5	127	0.4 ± 0.004	0.1 ± 0.001	0.1 ± 0.001	0.3 ± 0.003	1.2 ± 0.012
20–30	23	45	31	0.2	4.3	3.4	138	0.6 ± 0.006	0.1 ± 0.001	0.1 ± 0.001	0.3 ± 0.003	2.5 ± 0.025
30–40	27	44	29	0.3	4.5	3.4	156	0.8 ± 0.008	0.2 ± 0.002	0.1 ± 0.001	0.3 ± 0.003	2.7 ± 0.027
40–50	26	44	30	0.0	4.6	3.4	125	1.4 ± 0.014	0.2 ± 0.002	0.1 ± 0.001	0.3 ± 0.003	2.3 ± 0.023
50–60	30	41	30	0.1	4.9	3.5	98	2.6 ± 0.026	0.5 ± 0.005	0.1 ± 0.001	0.3 ± 0.003	1.3 ± 0.013

† Total organic C by wet digestion; precision of method ±4% (Chan et al., 1995).

‡ Soil pH in water and 1 mol L^{-1} KCl, respectively; instrumental error, according to manufacturer, of ±0.01 pH units.

§ Electrical conductivity.

¶ Mean ± SD.

removing the soil organic matter (Gee and Bauder, 1986). The soil pH was measured in deionized water (pH_w) and in 1 mol L^{-1} KCl (pH_K) (1:5 [w/v] suspension). Electrical conductivity was measured in a 1:5 (w/v) suspension. Total organic C (TOC) was determined by wet digestion (Walkley, 1934). Exchangeable bases were extracted with 1 mol L^{-1} NH_4OAc (at pH 7) (Thomas, 1982), and exchangeable Al was determined with 1 mol L^{-1} KCl (Barnhisel and Bertsch, 1982). Calcium, Mg, Na, K, and Al concentrations in extraction solutions were determined by inductively coupled plasma–atomic emission spectrometry (ICP–AES) on a PerkinElmer OPTIMA 4300DV (PerkinElmer Corp., Waltham, MA). Total Cu, Zn, and As for each 10-cm sample was determined by x-ray fluorescence on a Philips Magix spectrometer (Philips Analytical, Almelo, the Netherlands). Semiquantitative mineralogical composition of the total (≤2-mm) fraction of the soil was identified by powder x-ray diffraction (XRD) with a Philips PW-1710/00 diffractometer using the CuKα radiation with a Ni filter and a setting of 40 kV and 40 mA.

Dye Infiltration Study

A dye infiltration experiment was performed in December 2009 to visualize PF pathways at the experimental site. Brilliant Blue (BB) FCF (Color Index 42090) was used as the dye tracer (Flury and Flüher, 1995; Kasteel et al., 2007). Without any prewatering, a 6-cm front of dye solution (56 mm) containing 3 g L^{-1} of BB in fresh water was applied at a constant rate in an 80-cm-wide strip 1 m upslope from the sampling area for 1 h by means of an irrigation system consisting of four sprinklers, a dye reservoir, and an electrical vacuum pump. During the tracer application, both dye runoff and infiltration of the dye solution occurred within the experimental plot with an approximate surface area of 3 m^2.

Soil Sampling and Identification of Flow Domains

One day after the tracer application, the top 5-cm depth of soil was removed from the stream, and two parallel, vertical soil trenches (A and B) were consecutively excavated as shown in Fig. 1B. Once each profile was open, a 5-cm mesh was placed onto the open vertical surface. Soil samples were taken by pushing a cylindrical aluminum tube (5-cm length and 4.5-cm diameter) through the mesh into the soil wall, resulting in 128 samples (8 rows × 16 columns) per profile and a total of 256 soil samples (128 samples × 2 profiles). Based on visual examination of the open profiles in the stream and comparison of the analyses of in- and out-stream soil cores, two different layers could be defined within the experimental plot: the riverbed of the stream itself (RB) and the underlying B horizon of the natural subsoil (SS). The soil samples were classified into two groups corresponding to RB and SS, respectively, and samples were selected for the sequence of analysis shown in Fig. 2. After detailed visual examination, blue-stained samples were classified as PF domains and unstained samples were classified as soil MF domains. Samples taken from the interface of the layers were discarded. All samples were air dried and sieved through 2-mm mesh before further analysis.

Soil Analyses in Flow Domains and Sequential Extractions

Based on a stratified sampling procedure with simple allocation (profile, layer, flow domain), 10 soil samples were randomly selected within each stratum (80 samples total) (Fig. 2). Samples were dissolved in aqua regia (Chen and Ma, 2001) by microwave-assisted digestion (Ethos One, Milestone Srl, Sorisole, Italy), and solutions from the digestion were filtered and analyzed for total As, Cu, Zn, and S by ICP–AES on a PerkinElmer Optima 4300DV. The poorly crystalline and amorphous Fe fraction

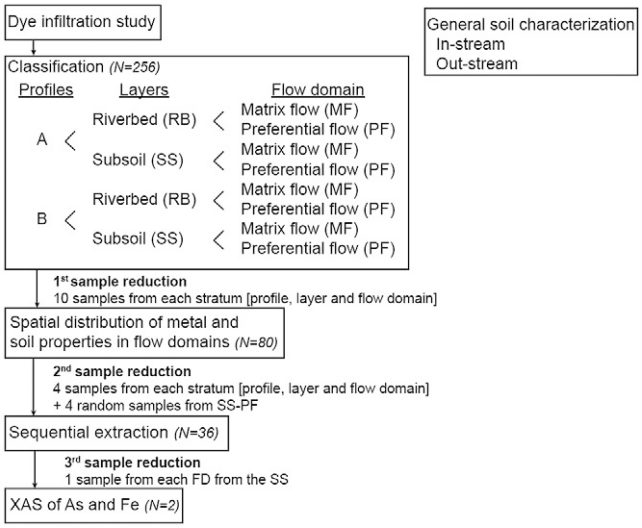

Fig. 2. Outline of experimental design, summary of sample collection and classification by profile, layer, and flow domain (FD), and stepwise analyses.

(Fe_{ox}) and the Fe content in the crystalline fraction (Fe_d) were determined as described in Shuman (1985) and Loeppert and Inskeep (1996), respectively. The pH_w, TOC, and concentration of exchangeable bases and Al were determined as described above.

Based on the distribution of As in the first sample set above, samples with As concentrations in the first and third quartiles, two samples closest to the median As concentration, and four random samples classified as SS-PF were selected for further analysis (36 samples total) (Fig. 2). Statistical analyses (Receiver Operating Characteristic curves) showed that the non-normal distributions of total metal(loid) concentrations, pH, TOC, and Fe_{ox} were not significantly different between the first (n = 80) and second (n = 36) sample sets. Samples were subjected to a three-step sequential chemical extraction scheme proposed by the Standards Measurement and Testing Program (BCR method; Rauret et al., 1999): FI, the fraction extracted with 0.11 mol L^{-1} acetic acid, corresponding to water-soluble or weakly bound species; FII, the fraction extracted with 0.1 mol L^{-1} hydroxylamine hydrochloride at pH 2, targeting poorly crystalline or reducible Al, Fe, and Mn (hydr)oxides; and FIII, the fraction extracted in 30% H_2O_2 oxidation and 1 mol L^{-1} NH_4OAc, targeting organic matter or oxidizable phases. The residual fraction (R) was sequentially measured for total metal concentrations after the FIII extraction using microwave-assisted digestion as described above.

Statistical Analyses of Soil Data

Differences in soil parameters with respect to flow domain were analyzed within each soil layer (RB or SS) using a generalized linear model (GLZ), with the presence or absence of dye (PF or MF) as a fixed principal factor and profile depth as a controlling covariate and assuming a Tweedie probability distribution for all variables. Similarly, soil parameters from the two soil layers were compared within each flow domain on the basis of a GLZ, with soil layer as the fixed principal factor and profile depth as a controlling covariate, assuming the same probability distribution for all variables. Within-domain spatial variability of the mean metal(loid) concentrations was initially assessed by means of the corresponding coefficient of variation (CV) of the concentrations as calculated by dividing the mean values by their standard deviations. Last, the characteristic multielemental composition of the flow domains was studied by means of multivariate analytical techniques based on neural networks for each layer by setting the flow domain (PF or MF) as the dependent variable (Fine, 1999; Ripley, 1996). The calculated global loadings on the dependent variable (flow domain) from the corresponding synaptic weights of each variable were used to identify multielemental relationships with both flow domains. To explain the association of solid-phase metal distribution resulting from the BCR extraction procedure (operational fractions) and flow domains, one fixed factor (flow domain) and two covariables (depth and fraction $k - 1$) were considered within a GLZ with three effects (flow domain, depth, and fraction), assuming a Tweedie probability distribution for all variables. All statistical analysis was done using the software package IBM SPSS Statistics 19 (IBM Corp., Armonk, NY).

Arsenic and Iron X-Ray Absorption Spectroscopy of Soils

Within each flow domain (PF or MF) in the SS, a sample was selected for bulk synchrotron x-ray absorption spectroscopy (XAS) analysis. Ground samples were placed in Teflon holders and sealed with Kapton tape. Samples for Fe XAS were diluted ~50% (v/v) in BN. For the PF sample, an As K-edge spectrum was collected on the bending-magnet BM25A beamline (SpLine) at the European Synchrotron Radiation Facility [6 GeV, 100 mA, Si(111) monochromator crystals] in fluorescence mode using a 13-element Si(Li) solid-state detector with the sample at room temperature (RT) (16 scans averaged). For the MF sample, an As extended x-ray absorption fine structure (EXAFS) spectrum was collected in fluorescence mode on the wiggler beamline 4-1 at the Stanford Synchrotron Radiation Lightsource (SSRL) [3 GeV, 100 mA, Si(220) monochromator crystals] using a 13-element Ge detector with the sample held in a liquid He cryostat (5–20 K) (16 scans averaged). Iron K-edge spectra on the same samples were collected at the SSRL on either the wiggler beamline BL 4-3 [PF sample at RT, Si(111) monochromator crystals] or BL 4-1 (MF sample at cryogenic temperature) with a Lytle fluorescence detector (seven scans averaged for PF and four scans for MF). For all spectra, the incident x-ray beam was detuned to 30 to 50% of maximum intensity to minimize higher order harmonic reflections. No major differences in spectral features were noted between room- and low-temperature spectra. Spectra were calibrated by setting the energy of the first inflection on the main absorption edge of an As foil (=11867 eV) or Fe foil (=7112 eV).

Spectra were analyzed using the programs ATHENA (Ravel and Newville, 2005) for linear combination fits and EXAFSPAK (George and Pickering, 2000) for shell-by-shell fits. The background was subtracted using a linear fit through the pre-edge region and the Autobak routine in ATHENA for the spline fit through the EXAFS region. Arsenic x-ray absorption near edge

structure (XANES) spectra were fit by linear least squares combination fits of reference compounds to verify the As oxidation state. Arsenic EXAFS data were analyzed using the shell-by-shell method (k range = 2.0–12.5 Å^{-1}), with theoretical reference functions calculated by the program FEFF 8.0 (Ankudinov et al., 1998) based on atomic clusters from crystalline reference compounds calculated with the program ATOMS (Ravel, 2001). A triangular multiple scattering path among bonded As and O atoms, resulting from the high symmetry of arsenate tetrahedra, was included in the fit model in addition to single-scattering paths (Root et al., 2009). Interatomic distance (R), and either N (number of backscattering atoms) or σ^2 (the Debye–Waller factor), was treated as a variable parameter for each atomic shell. The threshold energy (E_0) was treated as a single variable for all shells, and the scale factor ($S_0{}^2$) was fixed (=1). Estimated errors based on empirical fits to reference compounds are: first shell, $R \pm 0.01$ Å, $\sigma^2 \pm 10\%$ (N fixed); greater than first shell, $R \pm 0.02$ Å; $N \pm 25\%$ (σ^2 fixed) (O'Day et al., 2004; Root et al., 2009).

Iron XANES and EXAFS spectra were fit by linear least squares combination fits using a well-characterized reference compound library (O'Day et al., 2004). The normalized XANES and k^3–weighted EXAFS regions of each spectrum were fit independently with a fixed energy scale. Initially for XANES fits, the entire library was screened to determine the combinations of reference spectra that best matched the data. From this analysis, a smaller set of compounds consisting of phyllosilicate and Fe(III) oxide minerals was selected, fit with all combinations of two or three spectral components, and ranked by statistical best fit. Finally, tests were performed with the highest ranking mixture of components to assess the sensitivity of the fit to the number of reference components, treating energy as a variable parameter and changing the spectral fit range. The sum of the reference components in the final fits was 100 ± 1.3%. Based on the results of the XANES analysis, linear least squares combination fits were done on the EXAFS spectra using the same set of reference spectra used for XANES. The proportions of components determined in the best fits were recalculated to 100%.

RESULTS

Soil Characteristics of the Experimental Site

Soil cores collected out of the stream bed showed that soils adjacent to the stream were characterized by a clay loam texture, alkaline pH_w (7.8–8.7), and low organic matter content (Fig. 3; Table 1). These soils have high effective cation exchange capacity (ECEC) and effective base saturation (>99.5%) but a low contribution from exchangeable Al^{3+} (<0.43%) to the ECEC (Table 1). In-stream soil, which receives run-off from the mine waste pile, was characterized by higher As concentration that decreased with depth, acid pH, and lower ECEC with a higher fraction of exchangeable Al^{3+} (Table 1; Fig. 3). Based on visual examination of the open profiles in addition to analyses of in-stream cores, two soil layers separated by a sharp interface could be distinguished in the stream—a riverbed and its subsoil (Fig. 4). The RB layer (0–20 cm) was characterized by a loam texture, higher organic matter, and acid pH compared with the SS (20–60 cm), which had a clay loam texture, lower organic matter, and acid pH (Table 1). Higher ECEC values, mainly associated with Ca^{2+} and Mg^{2+} and to some extent exchangeable Al^{3+}, were observed in the SS than the RB as a result of the higher clay content. Analysis of x-ray diffraction patterns of the RB soil showed hematite as the main crystalline Fe-bearing mineral phase, but hematite was not identified in the SS layer (Fig. 5). Finally, high concentrations of As, Cu, and Zn were found in both the RB and, to a lesser extent, the SS layer (Fig. 6), which is attributed to surface runoff from the waste pile and accumulation in the RB.

Water Flow Domains and Soil Properties

Figure 4 shows the heterogeneous dye distribution within one of the two open profiles. Stained areas were visible to the 45- to 50-cm depth. Both profiles showed similar distribution patterns, consisting of an upper layer of variable thickness that was heterogeneously stained and a deeper zone in which the infiltration front breaks into thin preferential paths and large portions of the soil matrix were bypassed. Dead and living roots and structural voids were associated with fast water and solute transport through PF within the SS layer. Detailed sampling of the profiles was used to differentiate the two flow domains, PF and

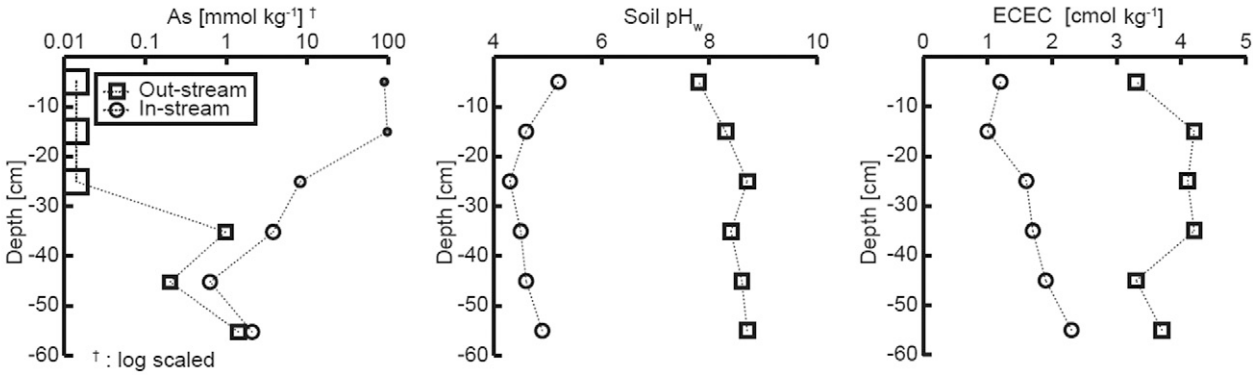

Fig. 3. Comparison of As concentrations, soil pH in water, and effective cation exchange capacity (ECEC) between samples from in-stream and out-stream soil cores.

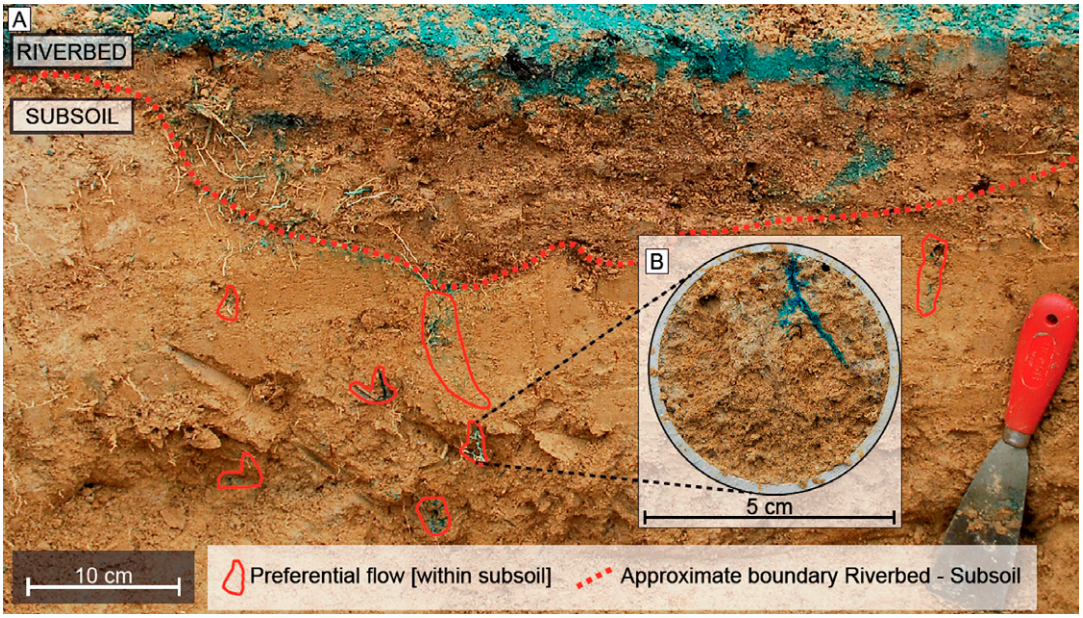

Fig. 4. (A) General view of the opened stained soil profile, and (B) magnified cross-section from one of the stained soil samples from the subsoil.

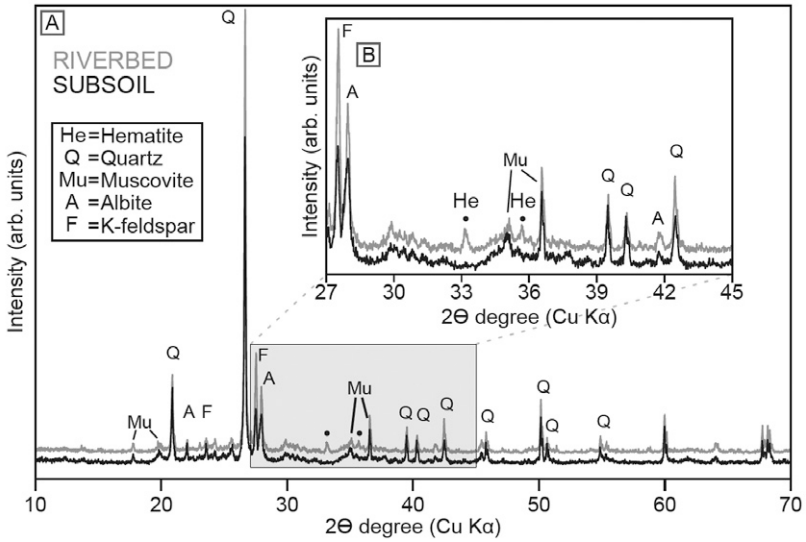

Fig. 5. (A) X-ray diffraction patterns of bulk samples from the riverbed (gray line) and the subsoil (black line), and (B) magnified section to emphasize the primary reflections from hematite in the riverbed sample.

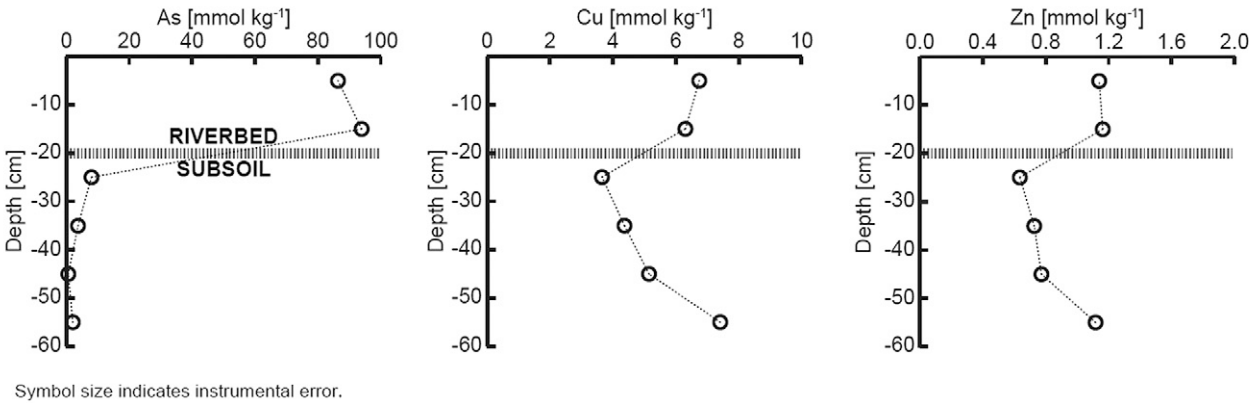

Fig. 6. Arsenic, Cu, and Zn concentrations as a function of soil depth from the surface within the stream bed. The dashed line marks the approximate transition from the riverbed to the subsoil. Arsenic data are replotted from Fig. 3.

Table 2. The pH and exchangeable cations from each soil layer and different flow domains.

Layer	Flow domain	pH_w†	Exchangeable cations				
			K^+	Ca^{2+}	Na^{2+}	Mg^{2+}	Al^{3+}
			$cmol_c\ kg^{-1}$				
Riverbed	Matrix flow	4.3 ± 0.1‡	0.2 ± 0.5	0.6 ± 3.0	0.1 ± 0.2	0.2 ± 1.1	1.5 ± 2.7
	Preferential flow	4.4 ± 0.1	0.2 ± 0.6	0.4 ± 1.5	0.0 ± 0.1	0.1 ± 0.4	1.0 ± 1.4
Subsoil	Matrix flow	4.1 ± 0.1	0.3 ± 0.2	0.7 ± 2.9	0.0 ± 0.1	0.3 ± 0.8	3.7 ± 3.7
	Preferential flow	4.0 ± 0.0	0.2 ± 0.5	0.6 ± 1.7	0.0 ± 0.1	0.2 ± 0.4	3.5 ± 3.8

† Soil pH in water; instrumental error, according to manufacturer, of ±0.01 pH units.

‡ Mean values (n = 80) ± standard error of the mean for pH in water and exchangeable cations in flow domains separated for the riverbed and subsoil layers.

Table 3. Trace metal concentrations, extractable Fe, and total organic C (TOC) from each soil layer and the different flow domains. Mean values (n = 80) and CV of Cu, Zn, As, and S, amorphous (Fe_{ox}) and crystalline (Fe_d) forms of Fe, and TOC in flow domains separated for the riverbed and subsoil layers.

Parameter	Matrix flow			Preferential flow		
	Mean	Median	CV	Mean	Median	CV
	$mmol\ kg^{-1}$					
	Riverbed					
Cu	7.38	6.10	34	8.70	8.55	31
Zn**	2.19	1.96	27	2.76	2.74	21
As*	72.00	60.42	64	103.70	96.95	48
S	24.55	20.80	55	29.14	27.98	43
Fe_{ox}	129.36	122.57	41	149.93	136.78	42
Fe_d	313.11	292.21	40	384.60	317.98	32
TOC**	0.11	1.00	54	0.83	0.75	70
	Subsoil					
Cu*	5.35	5.08	14	5.00	4.92	14
Zn**	2.19	2.14	16	1.94	1.93	12
As**	1.93	1.88	66	7.49	2.06	176
S*	11.96	11.01	48	19.48	17.16	60
Fe_{ox}**	57.74	57.87	25	76.28	74.69	28
Fe_d	117.56	117.61	24	116.17	111.98	17
TOC*	0.08	0.08	20	0.17	0.08	95

* Statistically significant differences between the two flow domains at $P \leq 0.1$ (generalized linear model).

** Statistically significant differences between the two flow domains at $P \leq 0.05$ (generalized linear model).

MF, in each layer. In both layers, PF paths had a similar pH to the MF soil but lower ECEC values (Table 2). Higher Fe_{ox}, Fe_d, and S concentrations were associated with PF paths compared with MF in both layers (Table 3). Differences among these three parameters were not significant in the RB layer but were significantly different with respect to Fe_{ox} and S concentrations in the underlying SS layer. Total organic C in the RB was lower in PF than MF samples, but the opposite trend was observed in the SS, with higher TOC in the PF than MF domains (Table 3).

Water Flow Domains and Metal(loid) Spatial Distribution

Within-domain spatial variability of the mean Cu, Zn, and As concentrations, as estimated by the CV, was different in the flow domains of the RB and SS layers. In the RB, the CV was relatively high overall for Cu, Zn, and As mean concentrations but higher in the MF samples than the PF samples (Table 3). Within the SS, the CVs for Cu and Zn means were low and similar in both MF and PF domains (~14%). The CV for the As mean concentrations was markedly different, changing from 65 to 176% in the MF and PF domains, respectively. This especially heterogeneous As spatial distribution in the PF domain of the SS layer was mainly due to the existence of two individual samples with high As concentrations (1190 and 1245 mg kg^{-1}) and two other samples, considered outliers, with As concentrations of 3670 and 4140 mg kg^{-1}, which markedly deviated from the interquartile range ($Q_3 - Q_1$) of the data distribution within this sample pool.

Neural network analysis was used to examine the multivariable elemental composition of the PF and MF flow domains within the RB and SS layers (Fig. 7). Neural networks provide a method to model complex or nonlinear relationships among data. This analysis produces a predictive model for a dependent or target variable (flow domain) based on the values of a series of predictor variables [metal(loid)s, Fe_{ox}, and TOC concentrations]. Briefly, a neural network usually consists of an input layer (predictor variables), a hidden layer, and an output layer. All interneuron connections between input and hidden layers, as well as hidden and output layers, have associated synaptic weights proportional to the strength of the connection. Two dimensions in the hidden layer were sufficient to extract the important features contained in the input data, which produced correct predictions of the resulting model in 84% of the test samples from both the RB and SS, and provided a measure of predictability in the multivariable space. The resulting neural network model includes all neuron layers and connections, with line thickness proportional to strength and the type of line indicating the operative sign (+ or −) (Fig. 7).

Global loadings calculated from the synaptic weights of the model are given in Table 4. Larger loading values for a given predictor indicate a greater association of that variable to either MF or PF domains. Accordingly, the PF domain in the RB was mainly characterized by higher Zn and lower TOC than the MF domain (Fig. 7A; Table 4). Arsenic association with the PF domain was not as strong as the other predictors, due mainly to its large spatial variability within this layer, although the model results are consistent with the higher mean concentration in the PF domain, as described by the univariate GLZ analyses.

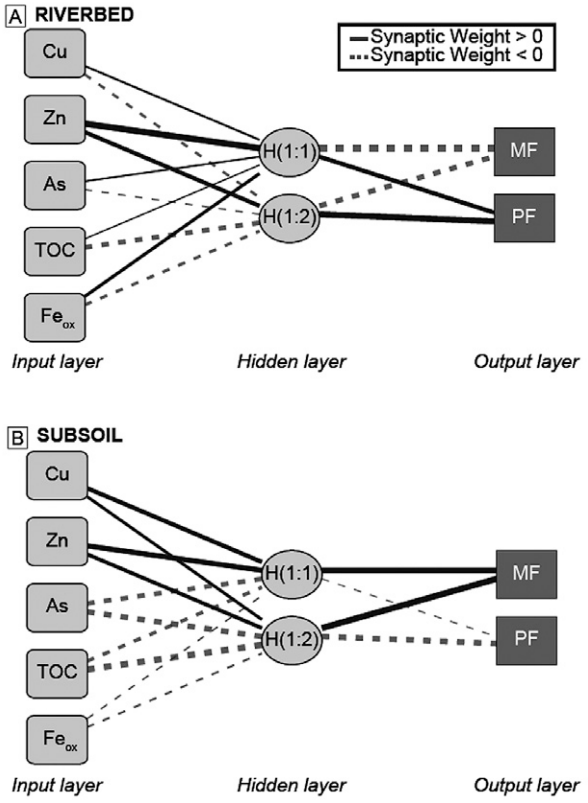

Fig. 7. Structure of neural network models for (A) riverbed and (B) subsoil layers. The input layer contains the predictor variables (Cu, As, Zn, total organic C [TOC], and amorphous Fe [Fe_{ox}]); the hidden layer contains the unobservable dimensions; the output layer (matric [MF] or preferential [PF] flow domain) contains the responses or dependent variables. Lines joining neurons represent synaptic weights, with strength proportional to the thickness of the lines; the type of line represents the operational sign of the interneuron connection (+ or −).

Neither Cu nor Fe_{ox} worked well as predictors and no association was found with flow domain. In contrast, in the SS layer, the characteristic chemical composition of the flow domains was more sharply differentiated than in the RB layer, i.e., all variables showed strong predictability for either PF or MF domain. In this case, both Cu and Zn were weak predictors, and As, TOC, and Fe_{ox} were stronger predictors, of the PF than the MF domain (Fig. 7B; Table 4).

Table 4. Global loadings of predictor variables on target variables (flow domains) from neural network models. Higher positive values indicate a higher degree of predictability of the soil concentration parameters for the flow domain (matrix flow or preferential flow)

Predictor	Target variable	
	Matrix flow	Preferential flow
Riverbed		
Cu	0.065	−0.659
Zn	−4.926	0.309
As	−0.246	−0.208
Total organic C	2.186	−2.399
Amorphous Fe	0.035	−0.700
Subsoil		
Cu	0.920	−0.460
Zn	1.388	−0.615
As	−1.807	1.303
Total organic C	−2.466	2.090
Amorphous Fe	−0.375	0.250

Solid-Phase Metal(loid) Extractability in Flow Domains

Metal(loid) distributions determined by the BCR sequential extraction method are shown in Fig. 8. In general, Cu, Zn, and As were found in the greatest proportion associated with the residual fraction (R) (26–74% of the total concentration) and to a lesser extent with the hydroxide or reducible fraction (FII) (9–34% of the total concentration). An exception is Cu in the SS layer, where it was associated mainly with the exchangeable or weakly bound fraction (FI) and with the poorly crystalline or reducible (FII) fraction rather than R.

With respect to flow domains, As and Cu were lower on average in R in the MF samples than the PF samples, and Zn was similar in both domains. Mean element concentrations in FII and FIII (associated with organic matter) fractions decreased slightly from the MF to PF domains. Minor differences were noted in the fraction targeting exchangeable species among samples. In the SS layer, the mean Cu and Zn concentrations in both flow domains followed similar trends to those in the RB layer. In contrast, As was higher in mean concentration in the PF than MF domain in all extraction steps except FI. The proportion of As in FI, FII, and FIII significantly increased and that of As in R significantly decreased from MF to PF domains (Fig. 8).

Arsenic and Iron X-Ray Absorption Spectroscopy in Subsoil Samples

Arsenic K-edge XANES spectra verified that As was present only as As(V) in both the MF and PF samples from the SS layer (Fig. 9A). The As XANES spectra of both soil samples could be fit with that of a reference spectrum of As(V) sorbed on ferrihydrite (molar Fe/As = 80) (Table 5). Fits to the As EXAFS spectra of the SS samples and the reference spectrum using shell-by-shell analysis resulted in an As–O first-shell coordination distance of 1.68 ± 0.01 Å ($N_{As\text{-}O}$ = 4, fixed), and two *s*-neighbor As–Fe distances (Table 5). Interatomic As–Fe distances for the PF spectrum were similar to that of the As–ferrihydrite spectrum, and $N_{As\text{-}Fe}$ (σ^2 fixed) was slightly lower than in the reference spectrum. For the MF spectrum, the best fits indicated a slightly shorter average As–Fe distance for the first Fe shell than found in the PF and reference spectra (3.31 ± 0.02 vs. 3.36–3.38 ± 0.02 Å). Interatomic As–Fe distances for the lower amplitude second Fe shell were slightly longer in the fit of the MF spectrum (3.55 ± 0.02 Å) than in the PF and reference spectra (3.51–3.52 ± 0.02 Å).

For the Fe X-ray absorption spectra, results from linear least squares combination fits indicated that both SS samples were dominated by a mixture of illite and smectite, with a smaller component of Fe(III) oxide that was best fit with a reference spectrum of ferrihydrite (Fig. 9B). Based on fits to XANES spectra, the MF spectrum had a smaller proportion

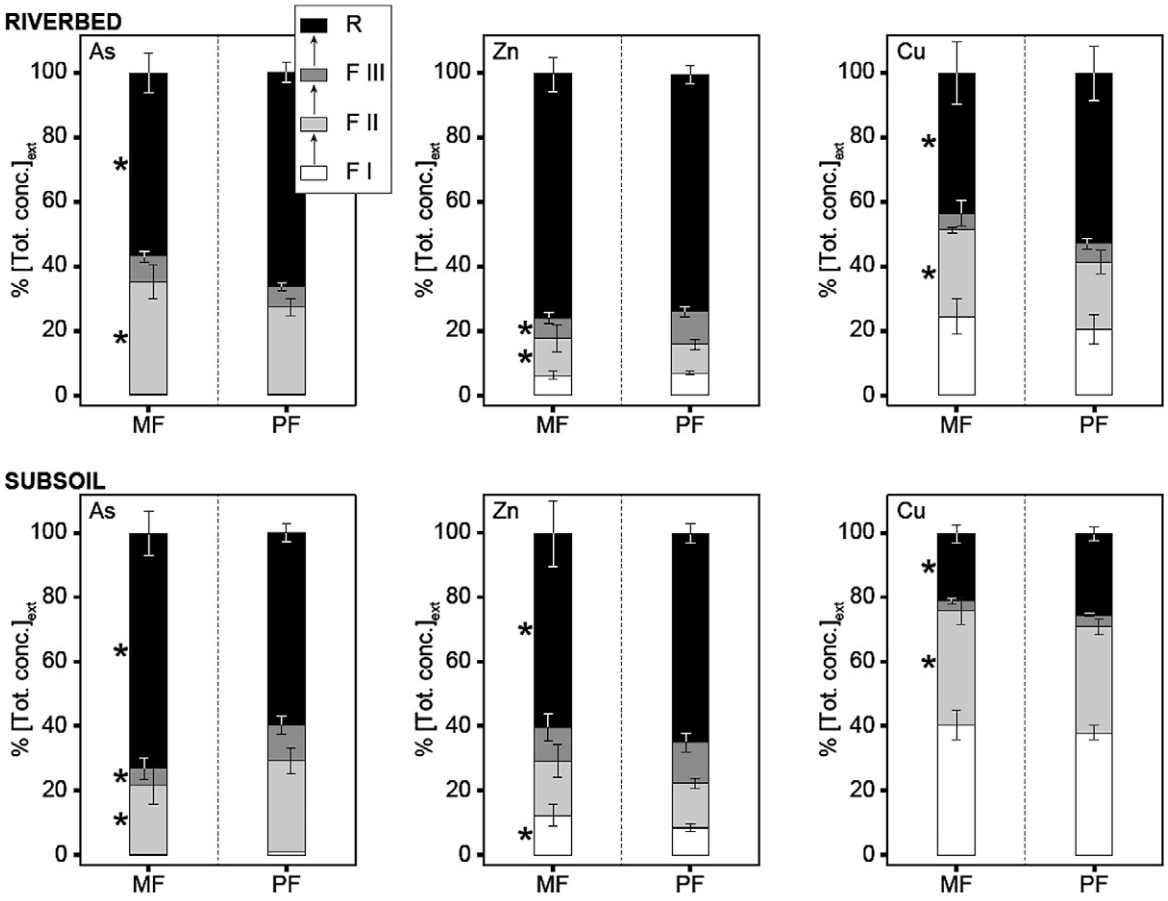

Fig. 8. Percentages of As, Zn, and Cu extracted with the easily soluble fraction (FI), reducible fraction (FII), oxidizable fraction (FIII), and residue (R) of the BCR extraction procedure (Rauret et al., 1999). Results are shown for soil horizons (riverbed and subsoil) and flow domains (matrix flow [MF] and preferential flow [PF]). *Statistically significant difference between the two flow domains at $P < 0.05$ (generalized linear model). Error bars represent the 95% confidence interval.

of ferrihydrite and more smectite than the PF spectrum, which was best fit with larger fractions of illite and ferrihydrite (Table 6). Linear combination (LC) fits of the Fe EXAFS spectra used the same reference components that were identified in the XANES analysis. In general, EXAFS LC fits tend to overestimate crystalline mineral fractions such as illite compared with amorphous phases such as ferrihydrite because of the stronger second-neighbor backscattering in crystalline materials (O'Day et al., 2004). As such, the fraction of ferrihydrite decreased in both samples in the EXAFS fits compared with the XANES fits, and the illite component was the dominant fraction in the EXAFS LC fits (Table 6). In results from both XANES and EXAFS fits, however, the PF sample contained about twice the amount of ferrihydrite as the MF sample.

DISCUSSION

Acidic Runoff and Soil Properties of the Riverbed

The overall soil characteristics found in the experimental site between the stream bed and outside of it reflect the local effect of seasonally intermittent runoff from the stock waste pile. During rainfall events, dissolution of scorodite present in the waste pile, associated with base consumption and proton generation as described in (Bluteau and Demopoulos, 2007), may lead to acidification and enhanced salt leaching within the stream channel compared with the adjacent soils. The acidity observed in the stream profile can also promote the destabilization of 2:1 clay minerals, resulting in a fraction of the Al^{3+} in octahedral layers becoming exchangeable, thus increasing the exchangeable acidity (Vazquez et al., 2011). A small fraction of hematite was identified by XRD in both the RB soil and a waste stock pile sample (data not shown) but not in the SS. The presence of a crystalline Fe oxide compound in the RB could be due to particle transport through surface runoff from the waste pile and accumulation in the upper stream soils or it could also be the transformation product of the previously precipitated ferrihydrite. Bulk As concentrations were particularly elevated in the top 20 cm of the stream profile compared with the out-stream soils (Fig. 3), which may have resulted from a combination of both dissolved and particulate As transport.

The Riverbed: A Transition Layer between Surface Runoff and Subsoil

Although staining-based experimental approaches provide no information on the origin of PF (Hagedorn and Bundt, 2002), visual evidence showed that nonequilibrium water infiltration conditions within the RB layer give rise to two flow domains, PF and MF. Differences in element concentrations and soil properties between the flow domains are probably the result of surface acid runoff and associated hyporheic exchange

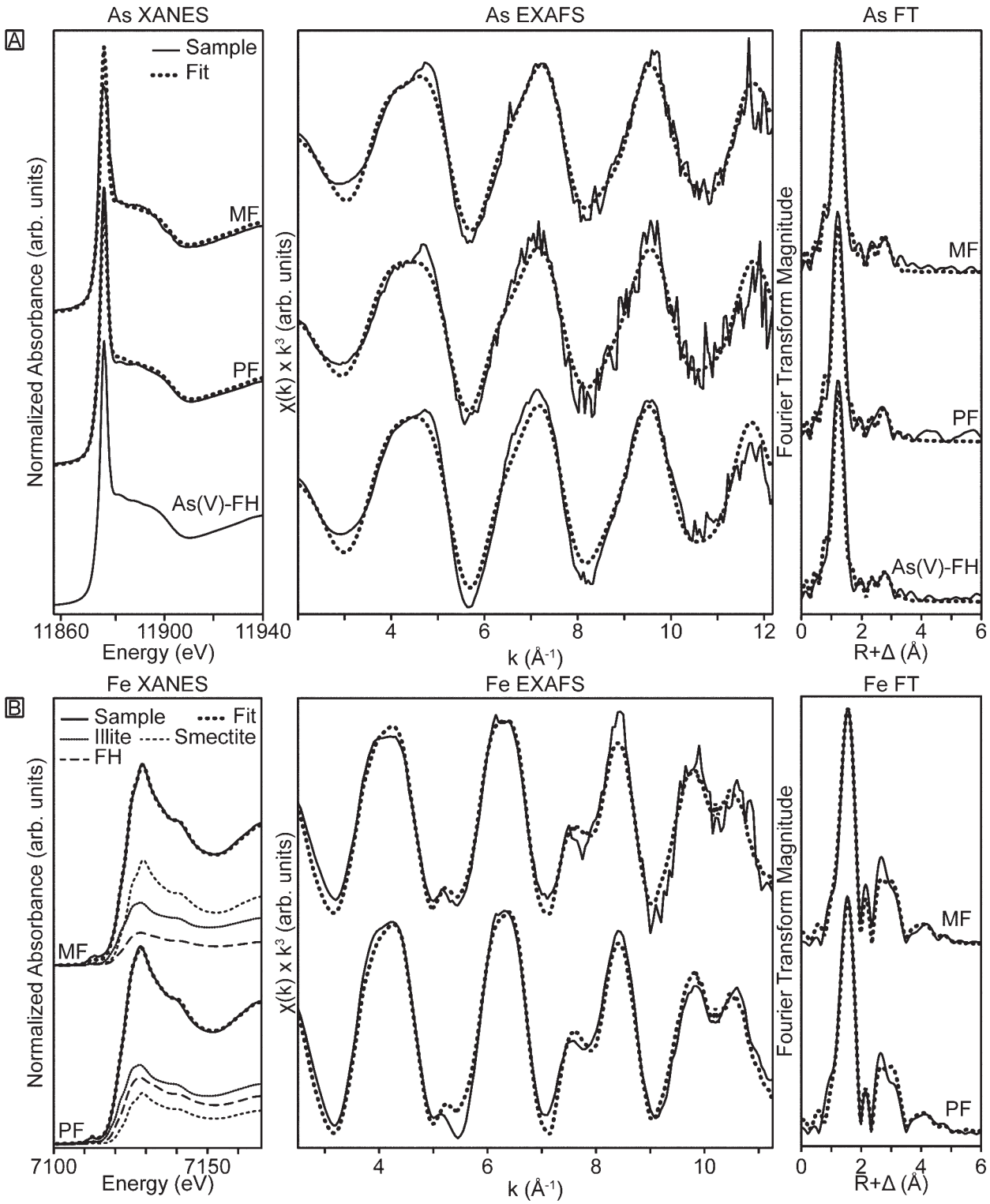

Fig. 9. (A) Arsenic and (B) Fe K-edge x-ray absorption near edge structure (XANES), extended x-ray absorption fine structure (EXAFS) and Fourier transforms (FTs) of subsoil sample spectra from matrix flow (MF) and preferential flow (PF) domains. The As XANES data were fit by a reference spectrum of arsenate sorbed to hydrous ferric oxide [As(V)-FH] (Root et al., 2009); As EXAFS were fit using a nonlinear least squares shell-by-shell approach. The Fe XANES and EXAFS spectra were analyzed by linear least squares combination fits with reference compound spectra of smectite (SWy-2), illite (IMt-1) (both from the Clay Minerals Society Source Clays Repository), and ferrihydrite (FH) (synthetic two-line ferrihydrite prepared following Schwertmann and Cornell, 2007). Numerical results are given for As in Table 5 and for Fe in Table 6.

in the stream channel, combined with preferential flow through the profile. Heterogeneity in flow can induce differences in soil properties and metal(loid) concentrations, although differences between the PF and MF domains in the RB layer were less distinct than those observed in the SS layer.

The results from statistical analyses (GLZ and neural network) showed no strong correlation trends between composi-

Table 5. Arsenic x-ray absorption near edge structure (XANES) and extended x-ray absorption fine structure (EXAFS) fits results.

Sample	As XANES†				As EXAFS§					
	As(V)-FH‡	Energy shift (ΔE)	Fitting range	Reduced χ^2	Atom	*N*	*R*	σ^2	ΔE_0	Reduced χ^2
	%	eV					Å	Å^2	eV	
Matrix flow	104.4	+0.4	11,857.5–11,940	3.34×10^{-3}	O	4.0	1.68¶	0.0021¶	−2.4¶	1.41
					MS#	1.0	3.06††	0.0032††		
					Fe	1.6¶	3.31¶	0.0060		
					Fe	1.1¶	3.55¶	0.0060		
Preferential flow	104.6	+0.4	11,857.5–11,940	6.08×10^{-3}	O	4.0	1.68¶	0.0022¶	−3.4¶	3.00
					MS#	1.0	3.05††	0.0031††		
					Fe	1.7¶	3.36¶	0.0060		
					Fe	0.8¶	3.51¶	0.0060		
As(V)-FH‡					O	4.0	1.68¶	0.0023¶	−2.4¶	1.44
					MS#	1.0	3.06††	0.0035††		
					Fe	1.7¶	3.38¶	0.0060		
					Fe	0.8¶	3.52¶	0.0060		

† Results from linear least squares fit of reference spectra. Goodness-of-fit was assessed by the χ^2 statistic [= (*F* factor)/(no. of points − no. of variables)].

‡ Arsenate sorbed to hydrous ferric oxide precipitated as two-line ferrihydrite previously analyzed by Root et al. (2009); used as reference for XANES fits of soil samples.

§ Results from nonlinear least squares shell-by-shell fit of theoretical referenced functions; *N* is the number of backscattering atoms at distance (*R*); σ^2 (Debye–Waller term) is the absorber–backscatterer mean square relative displacement (fixed σ^2 values for As–Fe shells from Root et al., 2009); ΔE_0 is the energy shift in the least squares fit; reduced χ^2 is a reduced least squares goodness-of-fit parameter [= (*F* factor)/(no. of points − no. of variables)]; scale factor (S_o^2) fixed at 1.

¶ Parameter allowed to vary during fit.

Spectrum fit with a multiple scattering path from As–O–O–As in arsenate tetrahedra (Root et al., 2009).

†† Parameter linked in fit to the parameter directly above.

tional variables and flow domains, with the exception of a positive correlation between Zn and the PF domain and a negative correlation between TOC and the PF domain. The total mean As concentration was much higher overall in the RB than in the SS layer but was not strongly associated with either PF or MF domains. Mean concentrations of amorphous and crystalline Fe were two to three times higher in the RB layer than the SS in both PF and MF domains (Table 3). Particle settling, filtration, and aggregation along variable paths within the porous RB, acting as a storage system, may explain the high mean concentrations of As and extractable Fe found in this layer and the reduced discriminator capacity of the selected soil properties to characterize flow domains. Percolation of acid water through the RB could increase leaching of exchangeable cations and dissolution of more soluble fractions at low pH, resulting in lower ECEC and TOC in PF domains. Particulate Fe oxide minerals may dissolve during acid infiltration and reprecipitate as amorphous Fe oxide. The results from sequential extractions showed a small increase in As and Cu associated with the residual fraction in the PF compared with MF samples. Dissolution of poorly crystalline phases in PF paths would tend to increase the fraction of metal(loids) in more recalcitrant phases.

Preferential Flow and Metal(loid) Speciation in the Subsoil

Visible structural features could be related to the observed dye pattern in the SS layer and analyses suggest that physical and chemical processes underlying nonequilibrium conditions in

Table 6. Iron x-ray absorption near edge structure (XANES) and extended x-ray absorption fine structure (EXAFS) fit results. Results from linear least squares fits of reference compounds. Goodness-of-fit was assessed by the reduced χ2 statistic [= (*F* factor)/(no. of points − no. of variables)].

Sample	Fitting range	Illite†	Smectite‡	Ferrihydrite§	Total	Reduced χ^2
	energy, eV	%				
Fe XANES						
Matrix flow	7118.1–7162	33.7	50.8	16.8	101.3	1.13×10^{-4}
Preferential flow	7118.1–7162	42.5	24.7	34.0	101.2	1.10×10^{-4}
	k, Å^{-1}	%				
Fe EXAFS						
Matrix flow	2.5–11.3	57	33	11	100¶	6.4×10^{-1}
Preferential flow	2.5–11.3	43	35	22	100¶	2.6×10^{-1}

† Fit with reference illite (IMt-1), Clay Minerals Society source clay mineral previously analyzed by O'Day et al. (2004).

‡ Fit with reference smectite (SAz-1), Clay Minerals Society source clay mineral previously analyzed by O'Day et al. (2004).

§ XANES fit by synthetic two-line ferrihydrite spectrum prepared following Schwertmann and Cornell (2007); EXAFS fit with ferrihydrite spectrum previously analyzed by O'Day et al. (2004).

¶ Recalculated to 100%.

water flow influence the spatial distribution of As, Cu, and Zn differently. Based on analyses of bulk in-stream cores, total Cu and Zn had similar concentration profiles and showed no trends with depth (Fig. 6). Neural network analysis showed that Cu and Zn were less strongly associated with PF paths than with the MF domain, but the opposite was observed for As, TOC, and Fe_{ox}. The mean TOC was lower in the SS than the RB, but TOC was a strong discriminator of PF paths in the SS. The fraction of As extracted in the FIII sequential extraction step (targeting organic matter and oxidizable phases) was higher in the PF (11%) than MF (5%) samples in the SS, although the amount of As extracted was much less than that associated with the poorly crystalline (FII) and residual fractions. The mean Zn concentrations were half as low as the mean Cu concentrations in the SS, but more Zn than Cu was associated with the residual recalcitrant fraction in the sequential extractions. X-ray absorption studies of Zn coordination in acid-impacted mine tailings showed that Zn in the recalcitrant sample fractions was associated with phyllosilicate and crystalline Fe oxide phases (Hayes et al., 2011). Results from the sequential extractions showed that Cu was mostly associated with easily exchanged and poorly crystalline soil fractions in PF and MF samples (>70%), reflecting its high mobility in both flow domains. Under acid conditions, Cu and Zn, as divalent cations, are expected to be mobile and may leach from the RB layer through PF paths into the MF domain of the SS if not incorporated into stable silicate or oxide phases. Sorption by Fe(III) oxides is a more important control on As mobility, particularly for As(V) as arsenate, than for Cu and Zn (Kumpiene et al., 2007), as confirmed by the results of the neural network analysis.

Spectroscopic results for As and Fe confirm the strong association of AsO_4^{3-} with Fe(III) oxide phases (Dixit and Hering, 2003; Stollenwerk, 2003). Interatomic distances and coordinating atoms determined from As EXAFS analysis for the PF sample are very similar to that of reference As(V) sorbed to synthetic ferrihydrite (Table 5) and in agreement with model studies of AsO_4^{3-} sorption to Fe(III) oxide minerals (Waychunas et al., 1993; Sherman and Randall, 2003). The As XAS results are consistent with the Fe XANES analysis of the PF sample, which showed an Fe(III) oxide component comprising 34% of the total Fe that was best fit with a ferrihydrite reference compound. Second-neighbor interatomic distances from As EXAFS for the MF sample were slightly different from those for the PF sample, and results from the Fe XAS analysis of the MF sample indicated a higher fraction of illite–smectite and less Fe(III) oxide (17% ferrihydrite from XANES). Minor differences in local As coordination between the PF and MF samples may have resulted from less dominance of amorphous Fe(III) oxides in the MF domain and greater variability in potential sorption sites for AsO_4^{3-}. Differences noted in the distribution of Fe phases determined by XAS correlate with a slightly lower mean extractable Fe oxide concentration (Fe_{ox}) for the MF than PF domains in the SS layer (Table 3).

Comparison of the chemical and spectroscopic results from the RB and SS layers suggests that Fe mobilized from the RB during acid flow may redistribute into the underlying SS through PF paths and precipitate as amorphous ferrihydrite. Discontinuities in PF paths, such as dead-end macropores (Allaire-Leung et al., 2000), may also contribute to enhanced, but heterogeneous, Fe(III) precipitation as an amorphous or poorly crystalline phase. The transfer of Fe from the RB into the SS through PF paths and higher abundance of amorphous Fe(III) oxide are consistent with the observed higher mean concentration of As in the PF samples and its heterogeneous spatial distribution, including the presence of a small population of samples with very high As concentrations. The correlation of PF paths in the SS with TOC may also suggest a role for organic matter in the retention of As (Sharma et al., 2010; Voegelin et al., 2007), although the mean TOC concentrations are very low. Whether PF paths in the SS are acting as both a sink for As and as a conduit for transfer into deeper soil horizons is difficult to assess because this experiment did not capture dynamic processes of the system. No evidence was observed in the soil profile, however, for reductive processes, such as the presence of As(III), Fe(II), or sulfide minerals, which would indicate mobilization of As from the reduction of As(V) or the reductive dissolution of Fe(III) oxides (Root et al., 2009; Hering et al., 2011). Based on the observations of this study, the seasonal dynamics of this system are probably dominated by a combination of surface flow and subsurface infiltration leading to alternating saturated and unsaturated conditions. Metal(loid) transport processes appear to be dominated by dissolution and precipitation of Fe(III) oxide phases for As as AsO_4^{3-} and pH-controlled sorption and desorption for Cu and Zn.

CONCLUSIONS

Differences in the flow regime in soils can play an important role in the distribution of metal(loid) contaminants through the interaction of physical and chemical processes. In prior studies, macropores have been considered "microsites" that are chemically more reactive than the surrounding matrix (Jarvis, 2007). In this study, we showed that PF paths subjected to intermittent infiltration of acidic water may behave as either conduits for element transfer or as local sinks, depending on the metal(loid) and the flow conditions. In soil samples from the RB, where both surface flow and subsurface infiltration occur, chemical differences between PF and MF regimes were not as distinct as in the subsoil. Soil chemical properties and metal(loid) distribution probably reflect variability among rainfall events, stream flow, and rates of subsurface infiltration that may create a broader distribution of flow regimes. In the subsoil, the mobility of Cu and Zn as divalent cations under acidic conditions is reflected in their distribution within the soil matrix rather than in PF paths. The association of As with PF paths containing more amorphous Fe(III) oxide than matrix soils can be interpreted as a consequence of the tight coupling of AsO_4^{3-} attenuation or mobilization to the precipitation and dissolution, respectively, of Fe(III) oxides that may occur during variable PF. Physical discontinuities within macropores, such as slow flow or dead-end pores, may act as traps for As and Fe and result in locally high concentrations within the subsoil. The erosion of the waste pile and surface transport leads

to an expansion of As and metal contamination through surface flow and potential particle transport. Mass transfer from the RB to the subsurface probably results from a combination of dissolution–precipitation and sorption–desorption processes related to acid leaching. The movement of As through PF paths may be retarded by adsorption on amorphous Fe(III) oxides, but this is a reversible process if geochemical conditions change. Although the results of this study present a temporally static view of the distribution of contaminants, there is evidence for an overall transfer of contaminants from storage in RB soils into the SS, where PF domains appear to act as conduits for metal transport and as both a source and a sink for As.

ACKNOWLEDGMENTS

This work was supported by the Spanish Ministry of Science and Innovation within the research project (CTM2006-00884) and by the U.S. National Science Foundation (NSF-EAR 0409203 to P. O'Day). The XAS measurements at the BM25A beamline were supported by the ESRF Project EC-649. The XAS data were collected at the Stanford Synchrotron Radiation Lightsource, a national user facility operated by Stanford University on behalf of the U.S. Department of Energy, Office of Basic Energy Sciences. M. Helmhart was supported by the CSIC Ph.D. fellowship program JAEPre (07-00272). P. O'Day was supported by the Spanish Sabbatical Programme (SAB2010-0133). We are grateful to Laura Barrios for her professional assistance with statistical analyses and to Javier Uruñuela for his help in field and laboratory work.

REFERENCES

Allaire-Leung, S.E., S.C. Gupta, and J.F. Moncrief. 2000. Water and solute movement in soil as influenced by macropore characteristics: 1. Macropore continuity. J. Contam. Hydrol. 41:283–301. doi:10.1016/S0169-7722(99)00079-0

Ankudinov, A.L., B. Ravel, J.J. Rehr, and S.D. Conradson. 1998. Real-space multiple-scattering calculation and interpretation of x-ray-absorption near-edge structure. Phys. Rev. B 58:7565–7576. doi:10.1103/PhysRevB.58.7565

Barnhisel, R., and P.M. Bertsch. 1982. Aluminum. p. 275–300. In A.L. Page et al. (ed.) Methods of soil analysis. Part 2. Chemical and microbiological properties. 2nd ed. Agron. Monogr. 9. ASA and SSSA, Madison, WI.

Bluteau, M.C., and G.P. Demopoulos. 2007. The incongruent dissolution of scorodite: Solubility, kinetics and mechanism. Hydrometallurgy 87:163–177. doi:10.1016/j.hydromet.2007.03.003

Bundt, M., A. Albrecht, P. Froidevaux, P. Blaser, and H. Flühler. 2000. Impact of preferential flow on radionuclide distribution in soil. Environ. Sci. Technol. 34:3895–3899. doi:10.1021/es9913636

Bundt, M., M. Jaggi, P. Blaser, R. Siegwolf, and F. Hagedorn. 2001a. Carbon and nitrogen dynamics in preferential flow paths and matrix of a forest soil. Soil Sci. Soc. Am. J. 65:1529–1538. doi:10.2136/sssaj2001.6551529x

Bundt, M., F. Widmer, M. Pesaro, J. Zeyer, and P. Blaser. 2001b. Preferential flow paths: Biological 'hot spots' in soils. Soil Biol. Biochem. 33:729–738. doi:10.1016/S0038-0717(00)00218-2

Bundt, M., S. Zimmermann, P. Blaser, and F. Hagedorn. 2001c. Sorption and transport of metals in preferential flow paths and soil matrix after the addition of wood ash. Eur. J. Soil Sci. 52:423–431. doi:10.1046/j.1365-2389.2001.00405.x

Camobreco, V.J., B.K. Richards, T.S. Steenhuis, J.H. Peverly, and M.B. McBride. 1996. Movement of heavy metals through undisturbed and homogenized soil columns. Soil Sci. 161:740–750. doi:10.1097/00010694-199611000-00003

Chan, Y.C., P.D. Vowles, G.H. McTainsh, D.D. Cohen, R.W. Simpson, and G.M. Bailey. 1995. Use of a modified Walkley–Black method to determine the organic and elemental carbon content of urban aerosols collected on glass fibre filters. Chemosphere 31:4403–4411. doi:10.1016/0045-6535(95)00308-U

Chen, M., and L.Q. Ma. 2001. Comparison of three aqua regia digestion methods for twenty Florida soils. Soil Sci. Soc. Am. J. 65:491–499. doi:10.2136/sssaj2001.652491x

Cheng, H.F., Y.N. Hu, J. Luo, B. Xu, and J.F. Zhao. 2009. Geochemical processes controlling fate and transport of arsenic in acid mine drainage (AMD) and natural systems. J. Hazard. Mater. 165:13–26. doi:10.1016/j.jhazmat.2008.10.070

Dixit, S., and J.G. Hering. 2003. Comparison of arsenic(V) and arsenic(III) sorption onto iron oxide minerals: Implications for arsenic mobility. Environ. Sci. Technol. 37:4182–4189. doi:10.1021/es030309t

Fine, T.L. 1999. Feedforward neural network methodology. Springer, New York.

Flury, M., and H. Flüher. 1995. Tracer characteristics of Brilliant Blue FCF. Soil Sci. Soc. Am. J. 59:22–27. doi:10.2136/sssaj1995.03615995005900010003x

Gee, G.W., and J.W. Bauder. 1986. Particle-size analysis, p. 383–411. In A. Klute (ed.) Methods of soil analysis. Part 1. Physical and mineralogical methods. 2nd ed. SSSA Book Ser. 5. SSSA, Madison, WI.

George, G.N., and I.J. Pickering. 2000. EXAFSPAK: A suite of computer programs for analysis of x-ray absorption spectra. Stanford Synchrotron Radiation Lab., Stanford, CA.

Ghodrati, M.D.C. 1992. A field-study of the effects of soil structure and irrigation method on preferential flow of pesticides in unsaturated soil. J. Contam. Hydrol. 11:101–125. doi:10.1016/0169-7722(92)90036-E

Hagedorn, F., and M. Bundt. 2002. The age of preferential flow paths. Geoderma 108:119–132. doi:10.1016/S0016-7061(02)00129-5

Hayes, S.M., P.A. O'Day, S.M. Webb, R.M. Maier, and J. Chorover. 2011. Changes in zinc speciation with mine tailings acidification in a semi-arid weathering environment. Environ. Sci. Technol. 45:7166–7172.

Hering, J.G., S. Hug, C. Farnsworth, and P.A. O'Day. 2011. Role of coupled redox transformations in the mobilization and sequestration of arsenic. p. 463–476. In P.G. Tratnyek et al. (ed.) Aquatic redox chemistry. ACS Symp. Ser. 1071. Am. Chem. Soc., Washington, DC.

Jarvis, N.J. 2007. A review of non-equilibrium water flow and solute transport in soil macropores: Principles, controlling factors and consequences for water quality. Eur. J. Soil Sci. 58:523–546.

Johnson, D.B., and K.B. Hallberg. 2005. Acid mine drainage remediation options: A review. Sci. Total Environ. 338:3–14. doi:10.1016/j.scitotenv.2004.09.002

Kasteel, R., P. Garnier, P. Vachier, and Y. Coquet. 2007. Dye tracer infiltration in the plough layer after straw incorporation. Geoderma 137:360–369. doi:10.1016/j.geoderma.2006.08.033

Knechtenhofer, L.A., I.O. Xifra, A.C. Scheinost, H. Flüher, and R. Kretzschmar. 2003. Fate of heavy metals in a strongly acidic shooting-range soil: Small-scale metal distribution and its relation to preferential water flow. J. Plant Nutr. Soil Sci. 166:84–92. doi:10.1002/jpln.200390017

Kumpiene, J., I. Castillo Montesinos, A. Lagerkvist, and C. Maurice. 2007. Evaluation of the critical factors controlling stability of chromium, copper, arsenic and zinc in iron-treated soil. Chemosphere 67:410–417. doi:10.1016/j.chemosphere.2006.08.031

Lennartz, B., N.J. Jarvis, and F. Stagnitti. 2008. Effects of heterogeneous flow on discharge generation and solute transport. Soil Sci. 173:306–320. doi:10.1097/SS.0b013e31816d1e8c

Lipsius, K., and S.J. Mooney. 2006. Using image analysis of tracer staining to examine the infiltration patterns in a water repellent contaminated sandy soil. Geoderma 136:865–875. doi:10.1016/j.geoderma.2006.06.005

Loeppert, R.H., and W.P. Inskeep. 1996. Iron. p. 639–664. In D.L. Sparks (ed.) Methods of soil analysis. Part 3. Chemical methods. SSSA Book Ser. 5. SSSA, Madison, WI.

Morales, V.L., J.-Y. Parlange, and T.S. Steenhuis. 2010. Are preferential flow paths perpetuated by microbial activity in the soil matrix? A review. J. Hydrol. 393:29–36. doi:10.1016/j.jhydrol.2009.12.048

O'Day, P.A., N. Rivera, Jr., R. Root, and S.A. Carroll. 2004. X-ray absorption spectroscopic study of Fe reference compounds for the analysis of natural sediments. Am. Mineral. 89:572–585.

Rauret, G., J.F. Lopez-Sanchez, A. Sahuquillo, R. Rubio, C. Davidson, A. Ure, and P. Quevauviller. 1999. Improvement of the BCR three step sequential extraction procedure prior to the certification of new sediment and soil reference materials. J. Environ. Monit. 1:57–61. doi:10.1039/a807854h

Ravel, B. 2001. ATOMS: Crystallography for the x-ray absorption spectroscopist. J. Synchrotron Radiat. 8:314–316. doi:10.1107/S090904950001493X

Ravel, B., and M. Newville. 2005. ATHENA and ARTEMIS: Interactive graphical data analysis using IFEFFIT. Phys. Scr. T115:1007–1010. doi:10.1238/Physica.Topical.115a01007

Recio-Vazquez, L., J. Garcia-Guinea, P. Carral, A.M. Alvarez, and F. Garrido. 2011. Arsenic mining waste in the catchment area of the Madrid detrital aquifer (Spain). Water Air Soil Pollut. 214:307–320. doi:10.1007/s11270-010-0425-x

Ripley, B.D. 1996. Pattern recognition and neural networks. Cambridge Univ. Press, Cambridge, UK.

Root, R.A., D. Vlassopoulos, N.A. Rivera, M.T. Rafferty, C. Andrews, and P.A. O'Day. 2009. Speciation and natural attenuation of arsenic and iron in a tidally influenced shallow aquifer. Geochim. Cosmochim. Acta 73:5528–5553. doi:10.1016/j.gca.2009.06.025

Schwertmann, U., and R.M. Cornell. 2007. Iron oxides in the laboratory: Preparation and characterization. Wiley-VCH Verlag, Weinheim, Germany.

Seo, Y., and J. Lee. 2005. Characterizing preferential flow of nitrate and phosphate in soil using time domain reflectometry. Soil Sci. 170:47–54. doi:10.1097/00010694-200501000-00006

Sharma, P., J. Ofner, and A. Kappler. 2010. Formation of binary and ternary colloids and dissolved complexes of organic matter, Fe and As. Environ. Sci. Technol. 44:4479–4485. doi:10.1021/es100066s

Sherman, D.M., and S.R. Randall. 2003. Surface complexation of arsenic(V) to iron(III) (hydr)oxides: Structural mechanism from ab initio molecular geometries and EXAFS spectroscopy. Geochim. Cosmochim. Acta 67:4223–4230. doi:10.1016/S0016-7037(03)00237-0

Shuman, L.M. 1985. Fractionation method for soil microelements. Soil Sci. 140:11–22. doi:10.1097/00010694-198507000-00003

Stollenwerk, K. 2003. Geochemical processes controlling transport of arsenic in groundwater: A review of adsorption. p. 67–100. In A.H. Welch and K.G. Stollenwerk (ed.) Arsenic in ground water. Kluwer Acad. Publ., Boston, MA.

Thomas, G.W. 1982. Exchangeable cations. p. 159–166. In A.L. Page et al. (ed.) Methods of soil analysis. Part 2. Chemical and microbiological properties. 2nd ed. Agron. Monogr. 9. ASA and SSSA, Madison, WI.

Toor, G.S., L.M. Condron, B.J. Cade-Menun, H.J. Di, and K.C. Cameron. 2005. Preferential phosphorus leaching from an irrigated grassland soil. Eur. J. Soil Sci. 56:155–167. doi:10.1111/j.1365-2389.2004.00656.x

Vazquez, O., J.D. Monnell, X. Pu, and R.D. Neufeld. 2011. Major processes dominating the release of aluminum from smectite clays when leached with acid mine drainage. Environ. Eng. Sci. 28:163–169. doi:10.1089/ees.2010.0195

Voegelin, A., F.-A. Weber, and R. Kretzschmar. 2007. Distribution and speciation of arsenic around roots in a contaminated riparian floodplain soil: Micro-XRF element mapping and EXAFS spectroscopy. Geochim. Cosmochim. Acta 71:5804–5820. doi:10.1016/j.gca.2007.05.030

Walkley, A. 1934. An examination of the Degtjareff method for determining soil organic matter, and a proposed modification of the chromic acid titration method. Soil Sci. 37:29–38. doi:10.1097/00010694-193401000-00003

Waychunas, G.A., B.A. Rea, C.C. Fuller, and J.A. Davis. 1993. Surface chemistry of ferrihydrite: 1. EXAFS studies of the geometry of coprecipitated and adsorbed arsenate. Geochim. Cosmochim. Acta 57:2251–2269. doi:10.1016/0016-7037(93)90567-G